VOL. 24, NO. 1, 2025, 7-13
elektrika.utm.my
ISSN 0128-4428

ELEKTRIKA
Journal of Electrical Engineering

CPW-fed Circular Patch Antenna with Rectangular Slot-Loaded DGS for Wideband Application

Mohamad Faiz Mohamed Omar[1,2], **Asrulnizam Abd Manaf**[2], **Mohd Fadzil Ain**[3,*] and **Sharul Kamal Abdul Rahim**[1,*]

[1]Wireless Communication Centre (WCC), Faculty of Electrical Engineering, Universiti Teknologi Malaysia, 81310, UTM Skudai, Johor, Malaysia.
[2]Collaborative Microelectronic Design Excellence Center (CEDEC), Sains@USM, Persiaran Bukit Jambul, 11900, Bayan Lepas, Pulau Pinang, Malaysia.
[3]School of Electrical and Electronic Engineering, Universiti Sains Malaysia, 14300, Nibong Tebal, Pulau Pinang, Malaysia.

[*]Corresponding author: eemfadzil@usm.my, sharulkamal@utm.my

Abstract: In this paper, a wideband circular patch antenna incorporated with a rectangular slot-loaded defective ground structure (DGS) is presented, meant for n77, n78, n79, and C band applications. The circular radiation patch of the proposed antenna is fed by a coplanar waveguide (CPW) mounted on a FR4 PCB board. At the bottom side of the board, a rectangular slot loaded on the DGS is added to establish good 50 Ω impedance matching and improve the antenna impedance bandwidth. This wideband antenna excites TM_{11} and higher-order TM_{21} modes at two distinct frequencies (3.3 GHz and 6.0 GHz). This circular patch antenna exhibits wideband behaviour with a fractional bandwidth > 90%, and an average efficiency of 76%.

Keywords: Coplanar waveguide, wideband, high efficiency, FR4 board, slot-loaded DGS

Article History: received 24 June 2024; accepted 12 December 2024; published 30 April 2025

1. INTRODUCTION

Wireless communication systems rapidly evolve due to the rising demand for different communication services. Future wireless communication technologies need smaller antennas and more bandwidth to accommodate data rate escalation [1, 2]. In this context, the design and dimensions of the antenna play a significant role in achieving a compact and miniaturised structure capable of working across a wide frequency range. Achieving a larger bandwidth with a smaller antenna dimension is tricky [3, 4]. A smaller volume dimension and wider bandwidth are unachievable using a typical antenna design formula, especially at low operating frequencies [5].

These days, microstrip patch antennas have evolved to the point where they are used in a wide range of industries and commercial applications. Thanks to their excellent attributes, including compact size, low profile, simplicity of integration with PCBs, and cheap manufacturing cost, which lead to large-scale production [6, 7]. Microstrip antennas' radiating patches come in a variety of shapes, including square, elliptical, rectangular, circular, and many more. Rectangular and circular patch antennas are among the most popular shapes due to their simple design and performance analysis [8, 9].

Theoretically, a circular patch antenna design is more straightforward by the fact that it just takes a single degree of freedom (radius) for its layout. Additionally, at the same design frequency, the circular patch antenna is ~16% more compact than the rectangular patch antenna [10]. Despite the fact that the microstrip patch antennas have been often used in wireless communication systems, they still suffer from a restricted bandwidth, low gain, and relatively large dimension at low frequencies. In recent years, a lot of studies have been conducted to address the drawbacks of the patch antenna. A number of good ideas have been put forward for enhancing the bandwidth size of a compact antenna.

Geeta Kalkhambkar et al. [11] developed a compact fractal antenna featuring a notch and a partial ground plane to boost wideband performance. Shereen Abdalkadum Shandal et al. [12] proposed a fractal rectangular microstrip antenna with a semi-elliptical partial ground plane to enhance bandwidth coverage while preserving the antenna's compact size. Ankush Kapoor et al. [13] demonstrated a technique to improve the bandwidth antenna through the use of a miniaturised printed antenna featuring an additional partially slotted ground plane. Chaitali Mukta et al. [14] introduced a circular patch antenna incorporating a square slot ground plane for bandwidth enhancement. A circular slot is added to the antenna patch with the goal of achieving a smaller antenna dimension than the conventional design.

Partial ground planes have proven successful in expanding the bandwidth of the patch antennas. However, the existing typical wideband rectangular and circular patch antenna fabricated on the FR4 board just able to yield a fractional bandwidth of up to ~30% [11-14]. Despite the wideband fractal antenna design having excellent wideband coverage (> 90%) and high efficiency, unfortunately, it is more complex and needs a high degree of precision for fabrication [15].

In this paper, we present a method to boost the antenna bandwidth while maintaining high efficiency by using a basic circular patch layout. On the FR4 PCB board, the integration of CPW with rectangular slot-loaded DGS facilitates the reduction of the antenna's effective permittivity to achieve wide frequency range operation. This antenna exhibits wideband behaviour with a fractional bandwidth > 90%, and an average efficiency of 76%.

2. ANTENNA GEOMETRY AND DESIGN

2.1 Antenna Geometry Design

A wideband antenna is designed on a FR4 lossy substrate with a relative permittivity (ε_r) of 4.3, loss tangent (tan δ) = 0.025 @ 10 GHz, and thickness (h) = 1.6 mm. The antenna has an overall dimension of 37 mm × 30 mm × 1.67 mm. The circular patch antenna geometry and its optimised parameter values are shown in Figure 1 and Table I, respectively.

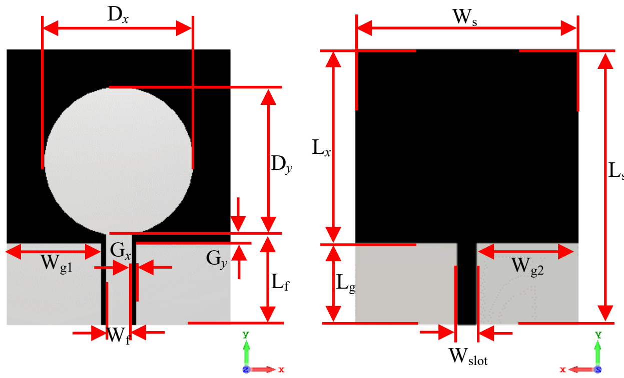

Figure 1. Geometrical configuration of the proposed wideband circular patch antenna.

Table 1. Dimension of parameters of the proposed antenna (mm)

W_s	L_s	L_g	W_{g1}	D_x	D_y	W_f
30	37	11	12.65	20	20	3.5
L_f	L_x	W_{slot}	G_x	G_y	W_{g2}	
12	26	3.5	0.6	1.0	13.25	

The proposed antenna configuration consists of a circular patch with a radius of 10 mm and a coplanar waveguide (CPW) that uses a conductive copper layer on the substrate's top surface. The effective radius (R_{eff}) of a typical circular-shaped radiator can be calculated using equation in (1).

$$R_{eff} = R\left\{1 + \frac{2h}{\pi\varepsilon_r R}\left[\ln\left(\frac{\pi R}{2h}\right) + 1.7726\right]\right\}^{\frac{1}{2}} \tag{1}$$

$$R = \frac{F}{\sqrt{1+\frac{2h}{\pi\varepsilon_r F}\left[\ln\left(\frac{\pi F}{2h}\right)+1.7726\right]}} \tag{2}$$

$$F = \frac{8.791 \times 10^9}{f_r\sqrt{\varepsilon_r}} \tag{3}$$

Here, R represents the physical radius of the radiator, ε_r denotes the relative permittivity of the substrate material, and h stands for the height of the substrate. The resonant frequency (f_r) can be determined by using the effective radius as defined in equation (4).

$$f_r = \frac{1.8412 \times c}{4\pi R_{eff}\sqrt{\varepsilon_r}} \tag{4}$$

c stands for the light's speed in free space, which is equal to 3×10^8 ms^{-1}. The copper (Cu) conductive layer has a conductivity of 5.8×10^7 S/m with a thickness of 35 μm. To achieve an impedance matching of 50 Ω, the microstrip feed line width is precisely tuned to 3.5 mm, the CPW groove spacing to 0.6 mm, and the width of the rectangular slot-loaded on the defective ground structure (DGS) to 3.5 mm. CST Microwave Studio is used to simulate the antenna design.

2.2 Evolution of Antenna Design

A number of stages of evolution of the wideband circular patch antenna have been illustrated in Figure 2. The simulation curve diagram for the reflection coefficient of the corresponding models is presented in Figure 3. The initial phase of the antenna design involves a circular patch radiator fed by a CPW with a full ground plane (CPWG). The 1st simulated antenna shows poor performance in the reflection coefficient due to a line impedance mismatch, which is far below 50 Ω. The next 2nd antenna structure keeps the CPW-fed circular patch design on the substrate's top surface, with a partial DGS supporting it at the bottom. The 2nd stage antenna works at two distinct frequencies, exhibiting the characteristics of a dual-band antenna. One at 3.1 GHz, operating between 2.7 GHz and 3.8 GHz, and the other at 5.9 GHz, operating between 5.2 GHz and 6.8 GHz. An optimised wideband antenna that is properly matched to 50 Ω impedance is presented in Figure 2(d). This antenna keeps a similar circular patch structure on the FR4's top surface while having a rectangular slot-loaded DGS at its bottom. The proposed antenna resonates at 3.3 GHz and 6.0 GHz, operating between 2.7 GHz and 7.2 GHz, offering a fractional bandwidth (FBW) of 90.9%.

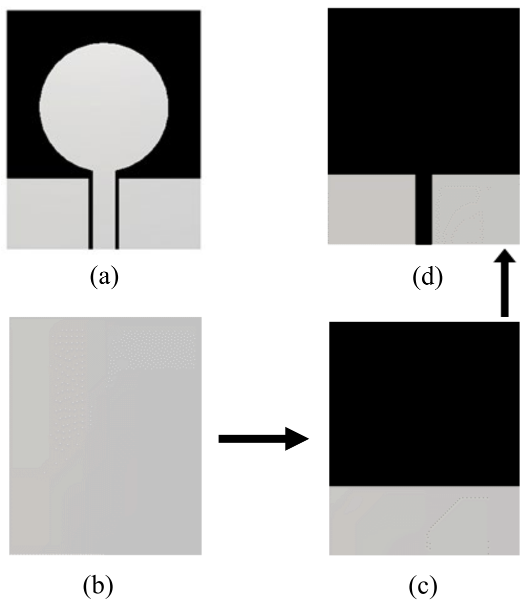

Figure 2. The antenna's evolution design stages.

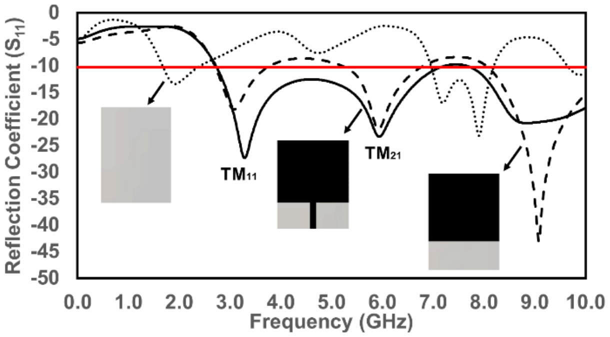

Figure 3. The simulation of the reflection coefficient of the antenna at different evolution stages.

Figure 4 demonstrates how the antenna's *E*-field gets excited when it works in the TM_{11} and TM_{21} modes from the perspective views. The *H*-field distributions as shown in Figure 5 are excited at the frequencies of 3.3 GHz and 6.0 GHz via the CPW feed line backed by the rectangular slot loaded on the DGS.

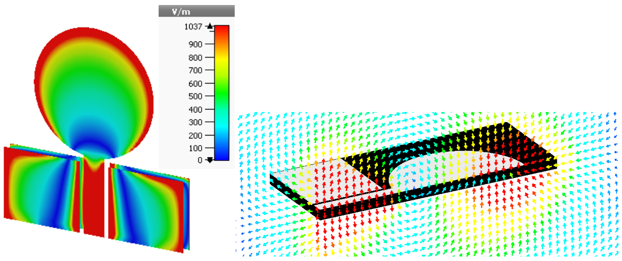

(a)

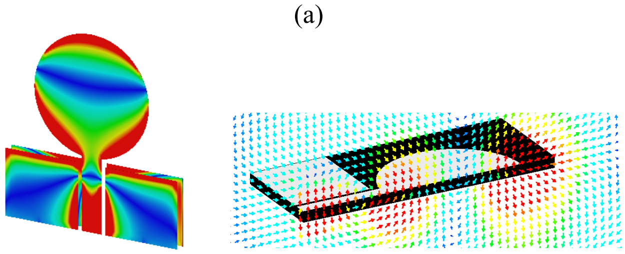

(b)

Figure 4. E-field of the proposed antenna at (a) 3.3 GHz and (b) 6.0 GHz.

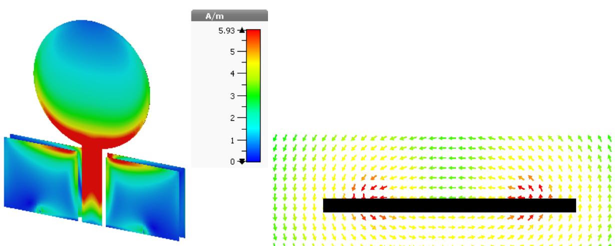

(a)

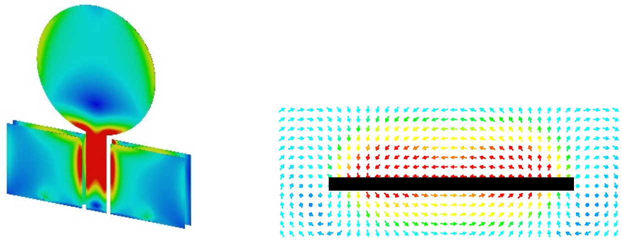

(b)

Figure 5. H-field of the proposed antenna at (a) 3.3 GHz and (b) 6.0 GHz.

The antenna's surface current distribution at 3.3 GHz and 6.0 GHz resonant frequencies is shown in Figure 6. By design, the proposed wideband antenna excites at two different order modes: TM_{11} and TM_{21}. The surface current distributions of the TM_{11} mode and higher-order TM_{21} mode are illustrated in Figures and, respectively. Here, a pretty even current distribution in each quadrant characterises the TM_{21} mode, in contrast to the elongated distribution found in the TM_{11} mode.

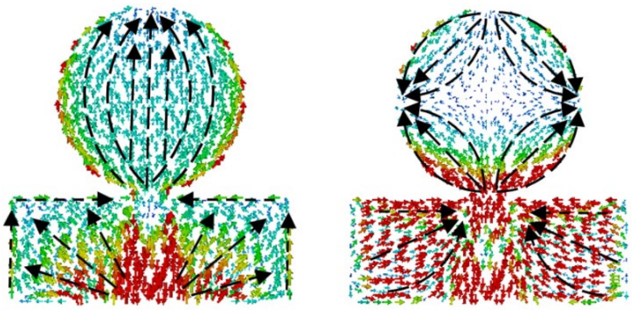

(a) (b)

Figure 6. Surface current distributions of the proposed antenna at (a) TM_{11} mode @ 3.3 GHz and (b) TM_{21} mode @ 6.0 GHz.

Figure 7 illustrates the effect of varying microstrip feed line (w_f) width on the S_{11} parameter at low and high resonant frequencies. As can be seen, increasing the width of the feed line results in a reduction of the impedance bandwidth. Expanding the microstrip line width brings the reflection coefficient closer to the -10 dB threshold line. It appears that the wideband behaviour switches to the dual-band as the width of the line hits 4.5mm. As a result, the impedance bandwidth worsens if the w_f increases further.

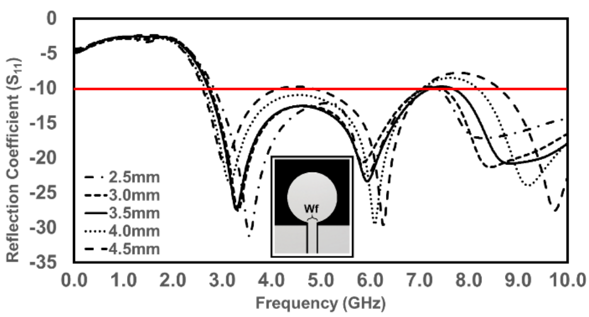

Figure 7. The simulation of the S_{11} parameter of the proposed antenna with different feed line widths (w_f).

Figure 8 unveils how the reflection coefficient of the wideband circular patch antenna changes with different CPW ground plane lengths (L_g), going from 7mm to 11mm with a step size of 1mm. It was found that increasing the length of the ground plane resulted in a slight upward shift in the resonant frequencies and a marginal enhancement in the impedance bandwidth. As expected, the variable L_g influenced the resonant frequency as well as the impedance matching of the antenna. Based on the S_{11} parameter's response, we can see that the impedance bandwidth expands when the CPW ground plane length closely matches the length of the feed line, with the feed line length set to 12 mm. In this case, the optimal dimension of the ground plane length is 11 mm, leaving a small gap of 1 mm between the far end of the circular patch and the ground plane.

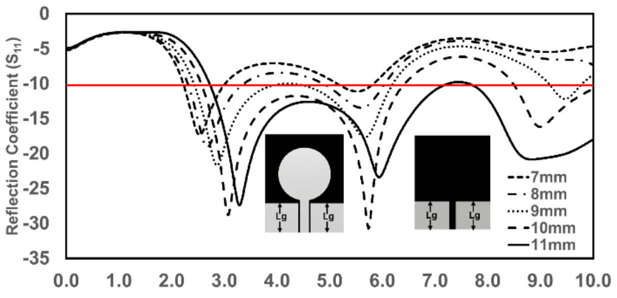

Figure 8. The simulation of the S_{11} parameter with different CPW ground plane lengths (L_g).

In Figure 9, the radius of the circular patch is set in the range between 6 and 10 mm to study the correlation between the patch radiator's dimension and the antenna's impedance bandwidth. A bandwidth size exceeding 4 GHz emerges when the radiator patch's radius reaches 9 mm, supported by TM_{11} and higher-order TM_{21} excitation modes. In this case, the largest fractional bandwidth (90.9 %) is earned when the circular patch's radius hits 10 mm.

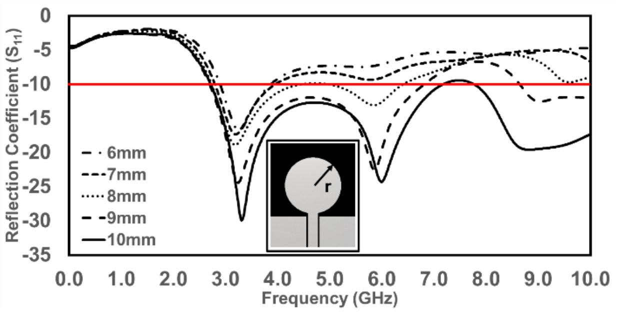

Figure 9. S_{11} simulated results with different circular patch radii (r).

The groove gap that exists between the feed line and the ground plane is seen to provide an additional bandwidth enhancement of the designed antenna. Based on the presented simulation in Figure 10, the gap size is sequentially increased in the step of 0.05 mm, ranging from the spacing of 0.5 mm to 0.7 mm. It seems that increasing the groove spacing results in a wider impedance bandwidth. The optimal gap size is found at 0.6 mm with an FBW increment of 2% by taking 0.5 mm gap spacing as the benchmark. However, increasing the gap beyond 0.6mm would subsequently lower the bandwidth owing to impedance mismatch exceeding 52.5 Ω.

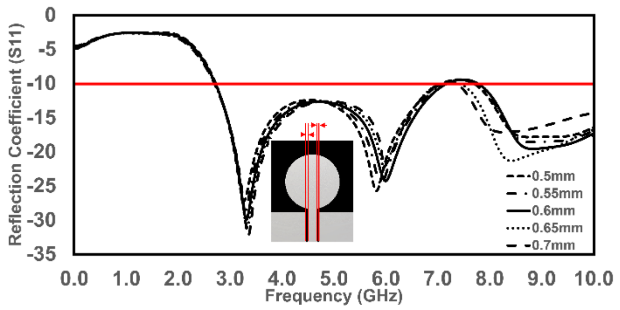

Figure 10. S_{11} simulated results with different groove spacing.

The bottom side of the antenna, which consists of a defective ground structure (DGS) coupled with a rectangular slot, is studied, aiming to further enhance the bandwidth size of the wideband operation on a FR4 substrate. The rectangular slot at the ground plane is added to facilitate a proper 50 Ω impedance matching in the presence of a 0.6mm groove gap. Incorporating a rectangular slot into the DGS structure keeps the dip resonant frequencies (f_{0L} and f_{0H}) below -20 dB. Figure 11 illustrates the reflection coefficient performances based on the rectangular slot width variations. It is clear that the impedance bandwidth increases whenever the width of the slot is increased. The optimal bandwidth size of the proposed antenna is achieved when the slot width is configured to be almost the same as the feedline while satisfying a 50 Ω impedance matching. In this case, it's possible to make the ground gap bigger than 3.5 mm, but that won't make the bandwidth bigger because the impedance matching will fail above 53 Ω.

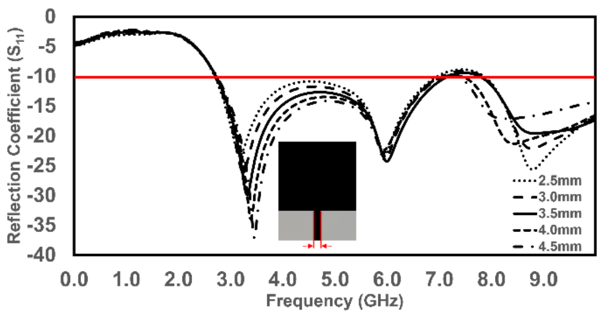

Figure 11. S_{11} simulated results with different rectangular slot widths on the DGS structure.

Figure 12 presents a comparison of the performance of the antenna's reflection coefficient (S_{21}) between the proposed CPW design with a rectangular slot-loaded DGS and the optimised conventional CPW design. The optimised standard CPW circular patch antenna is tuned to achieve a 50 Ω impedance matching by adjusting the groove spacing, to 0.34 mm while keeping the strip line width, Wf and circular patch size constant. From Figure 12, it is noted that the proposed CPW design with a rectangular slot-loaded DGS offers a larger impedance bandwidth and a 10.5% enhancement by taking the optimised standard CPW design as a benchmark. Adding a rectangular slot into the DGS structure affects the density of surface current distribution on the ground planes, leading to an increase in current flow through the circular patch, thus improving the impedance bandwidth. Besides, the conventional CPW structure also exhibits a slightly high permittivity, which is on average 29 % higher than the proposed antenna design structure, which negatively impacts the antenna impedance bandwidth.

Figure 13 illustrates the radiation patterns of the antenna in the elevation and azimuth planes at the resonant frequencies of 3.3 GHz and 6.0 GHz. Both diagrams (a) and (c) in Figure 13 visualise the simulated 3D plots of radiation patterns at 3.3 GHz with excellent omnidirectional. Stable broadside radiation patterns and directions are established across the operating frequency band. The radiation pattern of the proposed antenna at 6.0 GHz shows an omnidirectional-like pattern, as can be seen in diagrams (b) and (d).

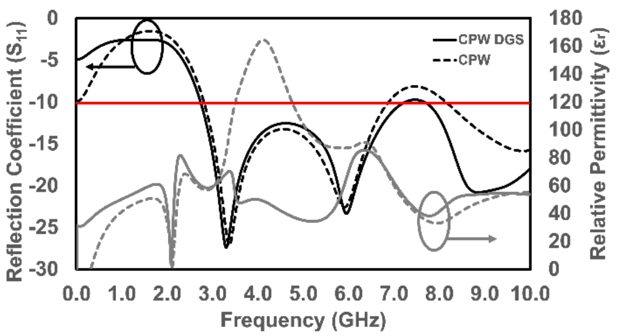

Figure 12. The comparison of simulated reflection coefficient (S_{11}) and relative permittivity (ε_r) behaviours between the conventional CPW antenna and the proposed antenna.

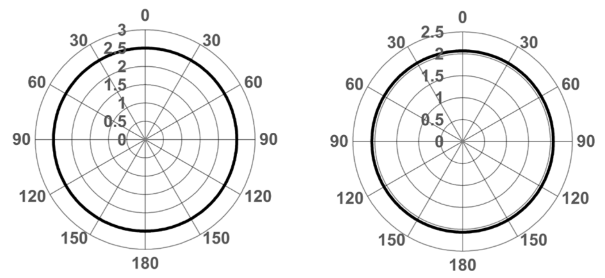

(a) *xz*-plane (b)

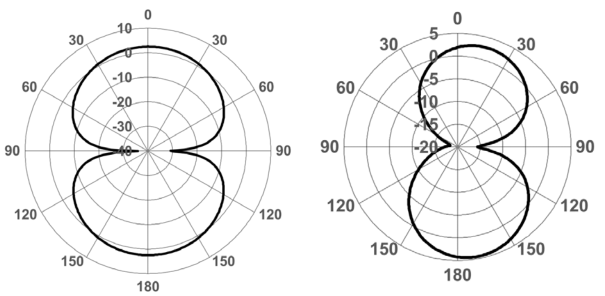

(c) (d)

yz-plane

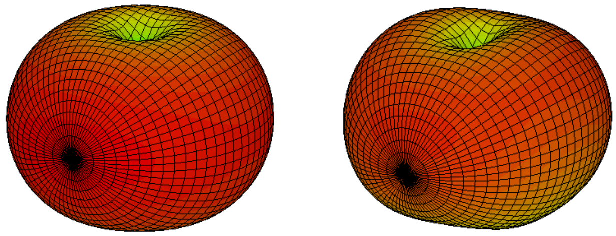

(e) (f)

Figure 13. The simulated radiation pattern at azimuth plane (a) 3.3 GHz (b) 6.0 GHz. The simulated radiation pattern at elevation plane. (c) 3.3 GHz (d) 6.0 GHz. (e) 3D radiation pattern plot @ 3.3 GHz. (f) 3D radiation pattern plot @ 6.0 GHz.

Figure 14 presents the proposed antenna's simulated gain as well as its radiation efficiency. The antenna offers a gain > 1.7 dBi across the passband. The maximum simulated gain is found to be 4.58 dBi @ 8.0 GHz. Based on the graph plotted in Figure 14, the simulated radiation efficiency is recorded to be higher than 81% within the operating band. At 7.5 GHz, the highest radiation efficiency is recorded to be 82.8%.

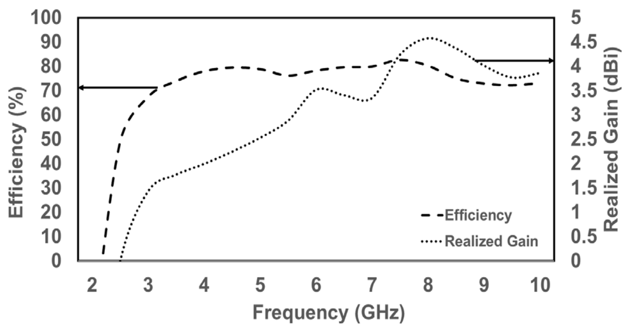

Figure 14. Simulation graph of both the radiation efficiency and gain for the proposed wideband antenna.

The fabricated wideband circular patch antenna prototype in Figure 15 is subjected to experimental validation to verify the simulated results. Both the simulated and measured return losses of the proposed antenna are shown in Figure 16, and it is noticed that there is a close degree of agreement between them. 90.9% of the simulated bandwidth is captured between 2.7 GHz and 7.2 GHz, with respect to the centre frequency at 4.95 GHz. The measured return loss yielded a fractional bandwidth of 72.73% from 2.8 GHz to 6.0 GHz, which is 18.17% narrower than the simulated bandwidth. According to Figure 16, the difference in the plotted results becomes noticeable at frequencies exceeding 5 GHz. This discrepancy is mainly due to the minor fabrication error and the significant loss of FR4 PCB at high-frequency bands.

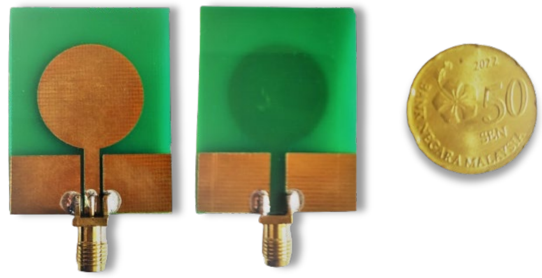

Figure 15. Photograph of the fabricated wideband circular patch antenna. (a) Front view (b) Rear view.

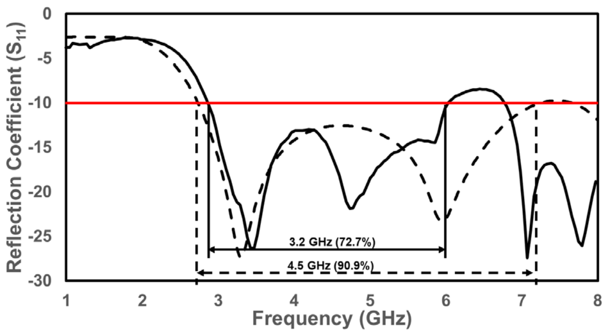

Figure 16. Simulated and measured return loss of the optimised wideband circular patch antenna.

3. CONCLUSION

In this paper, a compact wideband circular patch antenna designed on an FR4 lossy substrate is proposed. The proposed CPW-fed patch antenna is integrated with a rectangular slot-loaded DGS structure with the goal of enhancing the impedance bandwidth while keeping the size compact. On the FR4 PCB substrate, the circular patch antenna, with dimensions of $0.41\lambda_{0L} \times 0.33\lambda_{0L} \times 0.018\lambda_{0L}$, excites a TM_{11} mode at 3.3 GHz and a higher-order TM_{21} mode at 6.0 GHz with a simulated FBW of 90.9%. The wideband antenna offers a simulated gain > 1.7 dBi and an average efficiency of 76%. The measured return loss yielded a fractional bandwidth of 72.73% from 2.8 GHz to 6.0 GHz, which is 18.17% narrower than the simulated bandwidth. In the future, the proposed antenna will be considered to be designed and fabricated on the Rogers 4003C board to mitigate the significant loss caused by the lossy material.

ACKNOWLEDGMENT

This work was supported support from Ministry of Higher Education Malaysia and Universiti Teknologi Malaysia under Grant 4J611, 24H05, matching grant 04M57 4B888, 04M36, 4B856 and 4B777.

REFERENCES

[1] A. A. Abdulbari, Z. Zakaria, S. K. A. Rahim, Y. M. Hussein, M. M. Jawad, and A. M. Hamzah, "Design and development broadband monopole antenna for in-door application," *TELKOMNIKA*, vol. 18, no. 1, p. 51, Feb. 2020.

[2] M. F. M. Omar, S. K. A. Rahim, M. F. Ain, A. A. Manaf, and E.-H. Lim, "A Dual-Band Wideband Antenna on Thin Polyimide Film with Rectangular Slot-Loaded DGS," *in 2024 IEEE-APS Topical Conference on Antennas and Propagation in Wireless Communications (APWC)*, Sep. 02, 2024, pp. 79–83.

[3] K. V. Prashanth, P. M. Hadalgi, and P. V. Hunagund, "Survey on antenna gain and bandwidth enhancement techniques," *AIP Conference Proceedings*, vol. 2512, p. 020071, Jan. 2024,

[4] D. Zarifi, A. Farahbakhsh, and M. Mrozowski, "Improved Bandwidth of Microstrip Wide-Slot Antenna Using Gielis Curves," *IEEE Access*, vol. 12, pp. 74777–74783, Jan. 2024,

[5] L. Matta, B. Sharma, and M. Sharma, "A review on bandwidth enhancement techniques and band-notched characteristics of MIMO-ultra wide band antennas," *Wireless Networks*, vol. 30, no. 3, pp. 1339–1382, Nov. 2023.

[6] I. A. Zubir et al., "A Low-Profile Hybrid Multi-Permittivity Dielectric Resonator Antenna With Perforated Structure for Ku and K Band Applications," *IEEE Access*, vol. 8, pp. 151219–151228, Jan. 2020.

[7] M. F. M. Omar et al., "A critical review on the development of multi-geometrical stacked wideband dielectric resonator antenna," *Alexandria Engineering Journal*, vol. 100, pp. 111–141, Aug. 2024.

[8] M. F. Mohamed Omar, I. Ahmad Zubir, S. Kamal, and M. F. Ain, "A tri-hybrid of Al_2O_3-SiO_2-$MgZrO_3$ stair shaped half-cylindrical dielectric resonator antenna (SHCDRA) for wideband wireless communication systems," *Engineering Science and Technology, an International Journal*, vol. 35, pp. 1–10, 2022.

[9] S. K. Ezzulddin, S. O. Hasan, and M. M. Ameen, "Microstrip patch antenna design, simulation and fabrication for 5G applications," *Simulation Modelling Practice and Theory*, vol. 116, p. 102497, Apr. 2022.

[10] S. Kannadhasan and R. Nagarajan, "Performance Analysis of Circular Shape Microstrip Antenna for Wireless Communication System," *IOP Conference Series. Materials Science and Engineering*, vol. 1085, no. 1, p. 012013, Feb. 2021.

[11] G. B. Kalkhambkar, R. Khanai, and P. Chindhi, "A Novel Diagonally Symmetric Fractal Antenna with Wideband Characteristics for Internet of Things Applications," *Progress in Electromagnetics Research C. Pier C*, vol. 131, pp. 145–158, Jan. 2023.

[12] S. Shandal, Y. S. Mezaal, M. Kadim, and M. Mosleh, "New Compact Wideband Microstrip Antenna for Wireless Applications," *Advanced Electromagnetics*, vol. 7, no. 4, pp. 85–92, Sep. 2018.

[13] A. Kapoor, R. Mishra, and P. Kumar, "Compact wideband-printed antenna for sub-6 GHz fifth-generation applications," *International Journal on Smart Sensing and Intelligent Systems*, vol. 13, no. 1, pp. 1–10, Jan. 2020.

[14] C. Mukta, M. Rahman, and A. Z. Md. T. Islam, "Design of a Compact Circular Microstrip Patch

Antenna for WLAN Applications," *International Journal of AdHoc Networking Systems*, vol. 11, no. 03, pp. 01–11, Jul. 2021.

[15] A. Karmakar, "Fractal antennas and arrays: a review and recent developments," *International Journal of Microwave and Wireless Technologies*, vol. 13, no. 2, pp. 173–197, Jul. 2020.